

Detection of Gravitational Wave Emission by Supermassive Black Hole Binaries Through Tidal Disruption Flares

K. Hayasaki¹

Department of Astronomy and Space Science, Chungbuk National University, Cheongju 361-763, Korea

kimi@cbnu.ac.kr

and

A. Loeb

Harvard-Smithsonian Center for Astrophysics, 60 Garden Street, Cambridge, MA02138, USA

ABSTRACT

Galaxy mergers produce binaries of supermassive black holes, which emit gravitational waves prior to their coalescence. We perform three-dimensional hydrodynamic simulations to study the tidal disruption of stars by such a binary in the final centuries of its life. We find that the gas stream of the stellar debris moves chaotically in the binary potential and forms accretion disks around both black holes. The accretion light curve is modulated over the binary orbital period owing to relativistic beaming. This periodic signal allows to detect the decay of the binary orbit due to gravitational wave emission by observing two tidal disruption events that are separated by more than a decade.

Subject headings: accretion, accretion disks – black hole physics – gravitational waves – galactic: nuclei – hydrodynamics

1. Introduction

Most galaxies are inferred to harbor supermassive black holes (SMBHs) of masses in the range of 10^5 – $10^9 M_\odot$ at their center (Kormendy & Richstone 1995; Kormendy & Ho 2013),

¹Visiting Scholar, Harvard-Smithsonian Center for Astrophysics, 60 Garden Street, Cambridge, MA02138, USA

based on observations of stellar proper motion (Schödel, R. et al. 2002), stellar velocity dispersion (Magorrian et al. 1998) or accretion luminosity (Miyoshi et al. 1995). Cold gas triggers active galactic nuclei (AGNs) which produce intense radiation and powerful outflows in a minority of all galaxies, whereas the nuclei of most galaxies do not exhibit significant activities (Genzel et al. 2003).

Tidal disruption events (TDEs) provide a distinct opportunity to probe dormant SMBHs in inactive galaxies. Most TDEs take place when a distant star is perturbed into a parabolic orbit approaching close enough to the SMBH to be ripped apart by its gravitational tidal force (Rees 1988). The subsequent accretion of the debris stream of gas falling back to the SMBH produces a characteristic flare with a super-Eddington accretion rate for a timescale of weeks (Evans & Kochanek 1989). Recent observation of Swift J164449.3+573451 showed that relativistic jets are associated with some TDEs (Bloom et al. 2011; Burrows et al. 2011; Zauderer et al. 2011; Levan et al. 2011). Candidates for TDEs have also been observed at X-ray, ultraviolet, and optical wavelengths (Komossa & Greiner 1999; Gezari et al. 2012), although the observed light curves and spectra do not always match the simplest theoretical expectations (Gezari et al. 2012).

Binary SMBHs with a sub-parsec ($\lesssim 1$ pc) separation are considered to be the end product of a galaxy merger before the two black holes finally coalesce (Sillanpää et al. 1988; Graham et al. 2015). The merger of two SMBHs processes through three main stages (Begelman et al. 1980): first, the SMBHs sink towards each other via dynamical friction on the surrounding stars and gas. Once their separation drops below a parsec, a hard binary forms (Mayer et al. 2007) and tightens further due to other mechanisms until gravitational wave emission takes over (Colpi & Dotti 2011).

The observed TDE rate on single SMBHs is $\sim 10^{-5}\text{yr}^{-1}$ per galaxy (Donley et al. 2002; Velzen & Farrar 2014), although the recent theoretical works based on two-body relaxation imply the TDE rate could be one-order of magnitude higher (Wang & Merritt 2004). However, SMBH binaries are expected to exhibit an enhanced TDE rate of up to 10^{-1}yr^{-1} from chaotic orbital evolution and the Kozai-Lidov effect (Ivanov et al. 2005; Chen et al. 2009, 2011; Gongjie et al. 2015). Recent work suggests that multiple TDEs may occur in merging SMBH binaries with a rate of up to a few times over an observing period of five years with the *Large Synoptic Survey Telescope* (LSST)¹ (Wegg & Bode 2011).

Accretion disks around SMBHs are predicted to be gravitationally unstable at large radii where they fragment into stars or planets owing to their self-gravity (Paczynski 1978; Gammie 2001; Nayakshin et al. 2007). Similarly, a circumbinary disk could form stars in its

¹<http://www.lsst.org>

outskirts. Hence, a self-gravitating circumbinary disk would naturally lead to be an enhanced TDE rate (Amaro-Seoane et al. 2013). In addition, a circumbinary disk could grind the orbits of background stars and trigger additional TDEs (Miralda-Escudé & Kollmeier 2005). Through both mechanisms, stars would migrate to the inner edge of the circumbinary disk, and subsequently approach both black holes through the Lagrange points (L2 or L3) of the binary.

Here, we study how stars migrating through the binary Lagrange points are tidally disrupted by the SMBHs. In Section 2, we describe the numerical method used in our simulations of these TDEs. We then analyze our numerical results in Section 3. Finally, we summarize our main conclusions in Section 4.

2. Numerical model

We consider a system composed of a star orbiting around a circular SMBH binary with mass ratio $q = M_2/M_1 = 0.1$. The star originates from the massive circumbinary disk (Amaro-Seoane et al. 2013). The disk makes stars which migrate inwards and approach the Lagrange points around the binary (L2 or L3) via a mass stream from the disk’s inner edge (Hayasaki et al. 2007). The dynamics of the star can be treated as a restricted three-body problem. We solve numerically the motion of the star as a test particle in the binary potential.

In the test-particle limit, the star is initially located just inside the L2 point with a Keplerian velocity, and then is trapped by the binary potential and freely moves between two black holes inside the inner Roche-lobe of the binary. The outside of the inner lobe is marked by the shaded area of Figure 1 as the forbidden zone (Murray & Dermott 1999). The star is tidally disrupted once it enters the tidal disruption radius:

$$r_t \simeq \left(\frac{M_{\text{BH}}}{m_*}\right)^{1/3} r_* \sim 24 \left(\frac{M_{\text{BH}}}{10^6 M_\odot}\right)^{-2/3} \left(\frac{m_*}{M_\odot}\right)^{-1/3} \left(\frac{r_*}{R_\odot}\right) r_s, \quad (1)$$

where M_{BH} is the SMBH mass, m_* and r_* are the star’s mass and radius, and $r_s = 2GM_{\text{BH}}/c^2$ is the Schwarzschild radius. The corresponding orbit is depicted in Figure 1. The fate of the tidally disrupted star is similar to that of an eccentric TDE, in which the TDE accretion rate deviates significantly from the standard $t^{-5/3}$ time evolution (Hayasaki et al. 2013).

Our simulations are performed with a three-dimensional Smoothed Particle Hydrodynamics (SPH) code (Bate et al. 1995). The hydrodynamic equations are integrated using a second-order Runge-Kutta-Fehlberg integrator with individual time steps for each particle, leading to substantial savings in time for a large dynamic range of timescales. We also use

a variable smoothing length scheme to find the relevant spatial resolution in our code, but ignore the term proportional to the gradient of the smoothing length. We adopt standard the SPH artificial viscosity parameters $\alpha_{\text{SPH}} = 1$ and $\beta_{\text{SPH}} = 2$.

The photon diffusion timescale of the stellar debris is given by

$$t_{\text{diff}} = \frac{H}{c} \tau \simeq 6.1 \times 10^8 \left(\frac{\Sigma}{\Sigma_0} \right) \left(\frac{H}{\Delta r} \right) \left(\frac{r}{r_t} \right)^{-1} \text{ s}, \quad (2)$$

where H is the debris scale height and $\tau = \kappa_{\text{es}} \Sigma \sim 2.6 \times 10^6 (\Sigma/\Sigma_0)$ is the optical depth for electron scattering with $\kappa_{\text{es}} = 0.4 \text{ cm}^2 \text{ g}^{-1}$, and Σ is surface density of the stellar debris with the fiducial value of

$$\Sigma_0 \equiv \frac{m_*}{2\pi r \Delta r} \simeq 6.5 \times 10^6 \left(\frac{m_*}{M_\odot} \right) \left(\frac{r}{r_t} \right)^{-1} \left(\frac{\Delta r}{r_t} \right)^{-1} \text{ g cm}^{-2}, \quad (3)$$

where r and Δr are the radius and width of the debris ring. Recent three-dimensional radiation magneto-hydrodynamic simulations showed that the magnetic buoyancy induced through the magneto-rotational instability (MRI) (Balbus & Hawley 1991) provides an efficient radiative cooling mechanism for super-Eddington accretion flows (Jiang et al. 2014). In this regime, their preliminary simulations indicate that the radiative cooling speed is determined by the sound speed of the radiation. In our simulation, the stellar debris loses its orbital energy and then circularizes via a shock into an accretion flow at a super-Eddington rate at $\sim r_t$. The initial radiation energy density is $\sim \rho_0 v_t^2$, where $\rho_0 = \Sigma_0/r_t$ and $v_t = \sqrt{GM_{\text{BH}}/r_t}$, and so the radiation sound speed is estimated to be $c_{\text{s,rad}} \sim \sqrt{P_{\text{rad}}/\rho_0} \sim 0.08c$. Thus, the resulting cooling timescale $r_t/c_{\text{s,rad}}$ is estimated to be $\sim 2.8 \times 10^3 \text{ s}$, shorter than the heating timescale by the shock $2\pi\sqrt{r_t^3/GM_{\text{BH}}} \sim 10^4 \text{ s}$. It takes several dynamical times for the magnetic field to grow via the MRI, after which the efficient cooling reduces the thickness of the debris streams. Thus, we adopt a simple polytropic equation of state with $\gamma = 5/3$, which ensures that the radiative cooling is efficient, throughout our simulation.

We model the initial star as a polytropic gas sphere with $\gamma = 5/3$ in hydrostatic equilibrium. The star is set in motion through the gravitational field of the SMBH binary with the following parameters: $m_* = 1M_\odot$, $r_* = 1R_\odot$, $M_{\text{BH}} = 10^6 M_\odot$, $a = 100r_s$, and $q = 0.1$. The simulations follows 0.2 million SPH particles for 20 binary orbital periods, where a single period $P_{\text{orb}} \sim 1 \text{ day}$.

3. Tidal disruption of a star

Figure 2 shows the evolutionary sequence of density maps for the stellar debris of a TDE around the SMBH binary. A star approaching the binary from the L2 point is tidally

disrupted by the secondary black hole. Part of the stellar debris is not gravitationally bound, while the rest accretes onto the secondary SMBH. The unbound debris moves chaotically in the binary potential and forms accretion disks around both black holes by transferring mass along the potential valley through the L1 point.

The resulting mass accretion rates are shown in Figure 3A. The green and red dotted lines show the bolometric light curves of the primary and secondary black holes, respectively. The luminosities are derived as $L_{o,i} \propto \dot{M}_i c^2$ with $i = 1, 2$, where \dot{M}_1 and \dot{M}_2 are the mass accretion rates of the primary and secondary black holes based on the simulation. The accretion rates are estimated at the radius of the innermost stable circular orbit of a Schwarzschild black hole, $3r_s$. The black and blue lines show the bolometric light curves, including the relativistic doppler beaming effect due to the orbital motion of the binary (D’Orazio et al. 2015),

$$L_i = L_{o,i} \left[\frac{1}{\Gamma(1 - \beta_i)} \right]^4 \quad (i = 1, 2) \quad (4)$$

where $\Gamma = \sqrt{1 - (v_{\text{orb}}/c)^2}$ and $v_{\text{orb}} = \sqrt{GM/a}$ are the Lorentz factor and the orbital speed, respectively, and

$$\begin{cases} \beta_1 = (v_{\text{orb}}/c)(q/1 + q) \sin \theta_i \sin(\Omega_{\text{orb}} t) \\ \beta_2 = (v_{\text{orb}}/c)(1/1 + q) \sin \theta_i \cos(\Omega_{\text{orb}} t) \end{cases} \quad (5)$$

with $\Omega_{\text{orb}} = \sqrt{GM_{\text{BH}}/a^3}$ being the orbital frequency and θ_i being the inclination angle between the line-of-sight and the binary orbital plane, which is assumed to be $\pi/2$ in the calculation. Note that \dot{M}_1 intrinsically shows the bursty nature and is more than one order of magnitude smaller than \dot{M}_2 , since the angular momentum of the stellar debris relative to the primary black hole is much larger than that of the secondary black hole. In addition, the periodicity of the bolometric light curves of the secondary black hole is enhanced by relativistic beaming.

Figure 3B shows the power spectrum of the total light curve with relativistic beaming. The blue solid and red dashed lines mark the simulated and predicted power spectra, respectively. The blue line indicates a sharp peak at the binary orbital frequency. Since the full-width at half maximum of the peak is $\sim 0.029\Omega_{\text{orb}}$, the shift of the peak over time due to orbital decay should be larger than $\pm 0.03\Omega_{\text{orb}}$ in order to be easily noticeable. For a fiducial TDE rate of ~ 0.02 per year, a second TDE would likely occur 50 years after the first TDE, and the shift in the power spectrum due to the orbital decay by gravitational wave emission will be noticeable, as shown by the red dashed line of the figure. If the peak is sampled by N data points, then the shift in the peak would be detectable over a period shorter by

$\sim \sqrt{N}$. Our simulation implies that it would be possible to measure the orbital decay by gravitational wave emission through the shift of the peak in the power spectrum.

The TDE rate for a binary SMBH system is dictated by the supply rate of stars from the outer region of the circumbinary disk to the inner cavity. The formation rate of the solar mass stars is estimated to be of order $0.01 - 20 M_\odot \text{yr}^{-1}$ in the self-gravitating accretion disk (Nayakshin et al. 2007). The rate at which the orbits of disk-crossing stars are brought into the inner cavity could also be controlled by the mass accretion rate of the disk (Miralda-Escudé & Kollmeier 2005). In both cases, the stars should migrate to the inner cavity on the accretion timescale. Therefore, the expected TDE rate ranges between $\sim 0.01 \text{yr}^{-1}$ and the Eddington rate, $\dot{M}_{\text{Edd}}/M_\odot \sim 0.2 \text{yr}^{-1} (M_{\text{BH}}/10^6 M_\odot)(0.1/\epsilon)$, where ϵ is the mass-to-radiation conversion efficiency.

The feasibility of detecting the shift in the peak of the power spectrum depends primarily on the semi-major axis of the binary at the first TDE. We consider a circular binary whose coalescence timescale due to gravitational wave emission is given by (Peters 1964),

$$t_{\text{gw}} = \frac{5}{8} \frac{(1+q)^2}{q} \frac{r_{\text{S}}}{c} \left(\frac{a}{r_{\text{S}}} \right)^4 = \frac{5}{128} \frac{1}{\pi^{8/3}} \frac{(1+q)^2}{q} \left(\frac{r_{\text{S}}}{c} \right)^{5/3} P_{\text{orb}}^{8/3} \quad (6)$$

Setting a_0 and a as the semi-major axes of the binary at the first and second TDEs, respectively, the time difference between two TDEs, Δt_{gw} , needs to satisfy the condition that the normalized frequency is significantly increased, namely

$$\left(1 - \frac{\Delta t_{\text{gw}}}{t_{\text{gw}}(a_0)} \right)^{-3/8} \geq \frac{\Omega_{\text{orb}}}{\Omega_{\text{orb},0}} \quad (7)$$

Thus, the upper limit on a value of semi-major axis a_0 is,

$$\frac{a_0}{r_{\text{S}}} \leq \left[\frac{8}{5} \frac{q}{(1+q)^2} \frac{c}{r_{\text{S}}} \frac{\Delta t_{\text{gw}}}{1 - (\Omega_{\text{orb}}/\Omega_{\text{orb},0})^{-8/3}} \right]^{1/4}. \quad (8)$$

When t_{gw} is shorter than the viscous timescale evaluated at the inner edge of the circumbinary disk, the binary is viscously decoupled from the circumbinary disk (Milosavljević & Phinney 2005; Farris et al. 2015). The viscous timescale measured at the inner edge of the circumbinary disk is given by $t_{\text{vis}} = r^2/\nu$ with the inner radius being $\sim 2a$ (Artymowicz & Lubow 1994), where the disk viscosity $\nu = \alpha_{\text{SS}} c_{\text{s}} H$, expressed in terms of the sound speed c_{s} and the Shakura-Sunyaev viscosity parameter α_{SS} . Based on the assumption that the circumbinary disk is a standard disk, the decoupling radius is obtained by equating t_{vis} to t_{gw} , giving

$$\frac{a_{\text{dec}}}{r_{\text{S}}} = \left[\frac{2^{14/5} 5^{4/5} \sqrt{2}}{5} \left(\frac{c}{c_{\text{s},0}} \right)^2 \frac{q}{(1+q)^2} \right]^{5/13} \left(\frac{0.1}{\alpha_{\text{SS}}} \right)^{4/5} \left(\frac{M_{\text{BH}}}{M_\odot} \right)^{1/13} \left(\frac{\dot{M}}{\epsilon \dot{M}_{\text{Edd}}} \right)^{-2/13}, \quad (9)$$

where $c_{s,0} \sim 1.7 \times 10^8 \text{ cm s}^{-1}$ is the sound speed for typical parameters. Figure 4A shows the black-hole mass dependence of the decoupling radius. The decoupling radius is clearly larger than the fiducial semi-major axis $a_{\text{fid}} = 100r_{\text{S}}$ of our simulation for $10^5 M_{\odot} \leq M_{\text{BH}} \leq 10^8 M_{\odot}$. Because no significant binary-disk interaction occurs after decoupling, it is impossible for gas to accrete onto the SMBHs. However, dynamical friction between gas and stars near the inner edge of the circumbinary disk allows stars to lose their angular momenta and fall into the SMBHs (Ostriker 1999). This process would occur on the dynamical timescale, which is much shorter than the migration timescale of stars on the circumbinary disk, and so the TDE rate can be still comparable to the Eddington rate. Thus, a star can be supplied to a SMBH binary system at a high rate of up to 0.1 yr^{-1} (Chen et al. 2009), even if the system has no circumbinary disk because of a poor gas environment or because of decoupling.

The circumbinary disks can supply not only stars but also gas to the SMBHs before decoupling. Recent numerical simulations show that the rate of gas accretion from the circumbinary disk is modulated by the orbital period (MacFadyen & Milosavljević 2008; D’Orazio et al. 2013). Detection of the orbital decay based on the shift in the power spectrum of the light curves can also, in principle, be inferred in such a system. However, if the semi-major axis of the binary is larger than the decoupling radius, the shift of power spectrum is undetectable because it is too small to be identified observationally ($\Omega_{\text{orb}}/\Omega_{\text{orb},0} < 1.01$ in Figure 4B). This implies that only periodic signals caused by tidal disruption events around the SMBH binaries with the semi-major axis shorter than the decoupling radius can provide a detectable shift in the power spectrum.

4. Conclusion

We have simulated the tidal disruption of a star by a circular SMBH binary with a 1 : 10 mass ratio. Our simulation indicates that the mass accretion rate of the secondary black hole is higher than that of the primary black hole. The resulting total bolometric luminosity shows a strong relativistic beaming effect due to the enhanced line-of-sight velocity of the secondary black hole. Therefore, the power spectrum naturally shows a sharp peak at the orbital frequency (see Figure 3B). Observing two TDE flares separated apart by decades would allow to detect the orbital decay of the binary by gravitational wave emission.

Given that a typical galaxy encounters a merger with a mass ratio 1:10 once per ~ 1 Gyr (Wetzel et al. 2009), the probability for finding a corresponding SMBH binary in the last century of its life before coalescence is $\sim (10^2 \text{ yr}/10^9 \text{ yr}) \sim 10^{-7}$. The LSST will survey $\sim 2 \times 10^{10}$ galaxies for variability and be ideally suited for identifying candidate source for follow-up monitoring that will seek our predicted periodic signal.

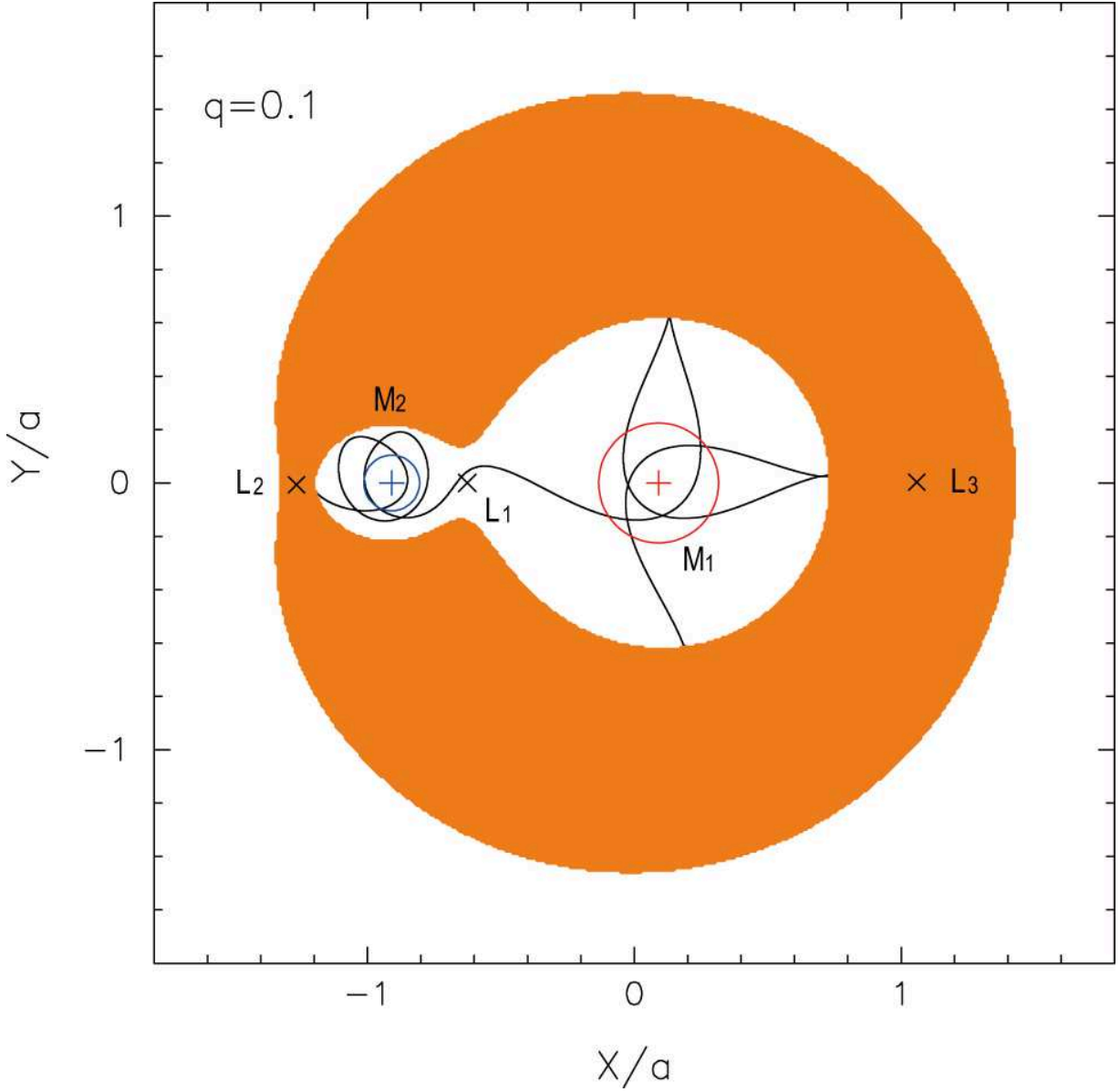


Fig. 1.— Orbit of a test particle in a co-rotating frame around a circular binary with $M_2/M_1 = 0.1$. The red and blue circles shows the tidal disruption radii around the primary and secondary black holes, respectively. The three black crosses mark the Lagrange points, L_1 , L_2 , and L_3 . Both axes are normalized by the binary semi-major axis. The black solid line shows the motion of a test particle inside the zero-velocity curve for a Jacobi constant $C_J = 3.45$, and the shaded area outside the curve denotes the forbidden zone (Murray & Dermott 1999).

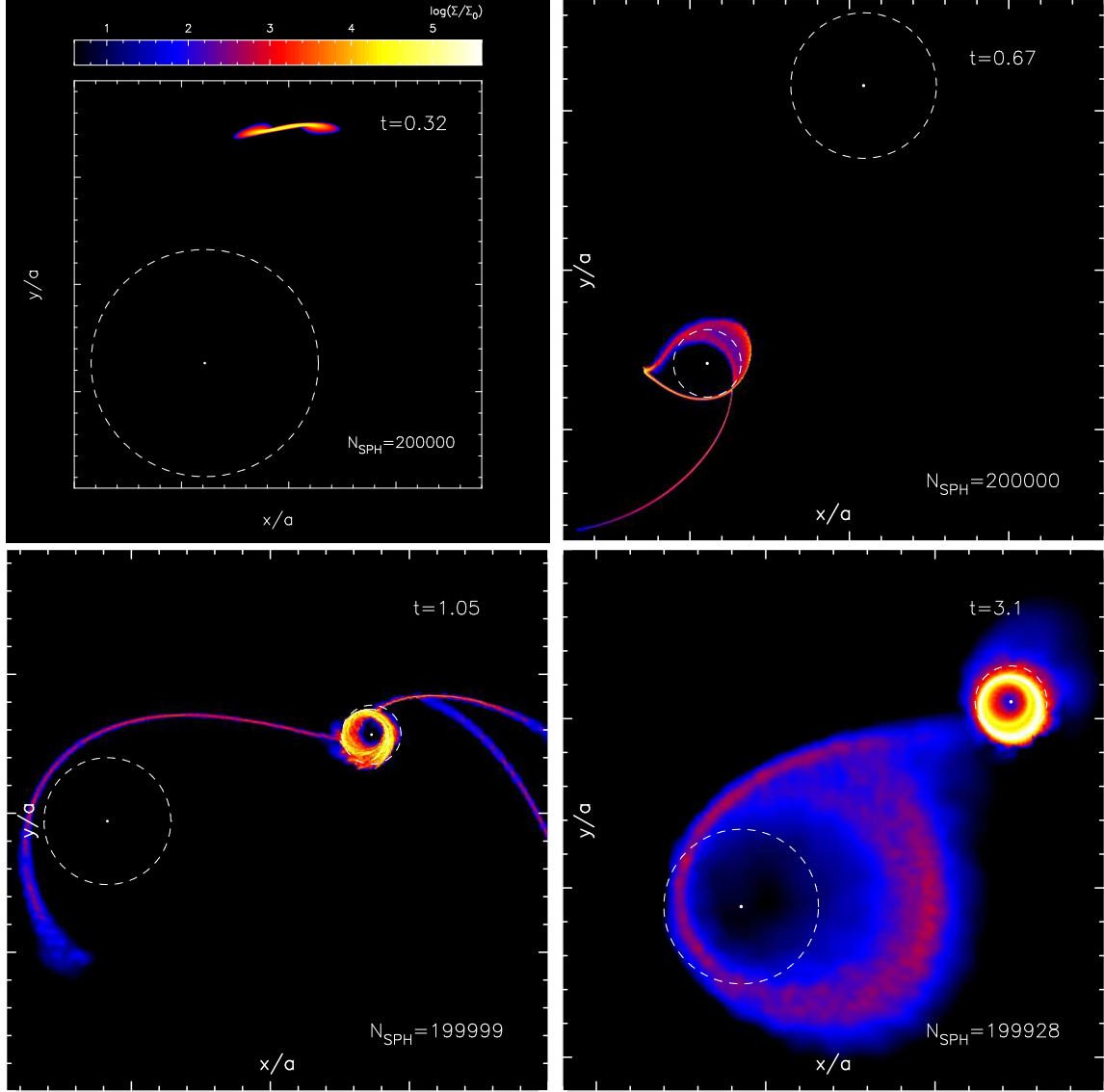


Fig. 2.— Gas density maps, projected on the orbital (x-y) plane, during a tidal disruption event in a circular SMBH binary with $M_{\text{BH}} = 10^6 M_{\odot}$, $a = 100 r_{\text{S}}$, and $q = 0.1$. The run time t is in units of P_{orb} as labeled in the top-right corner of each panel. The number of SPH particles is indicated at the bottom-right corner. The panels are shown in chronological order. The coloration indicates the density in five orders of magnitude on a logarithmic scale normalized by $\Sigma_0 = 6.5 \times 10^6 \text{ g cm}^{-2}$. The dashed circles indicate the tidal disruption radii for the primary and secondary SMBHs.

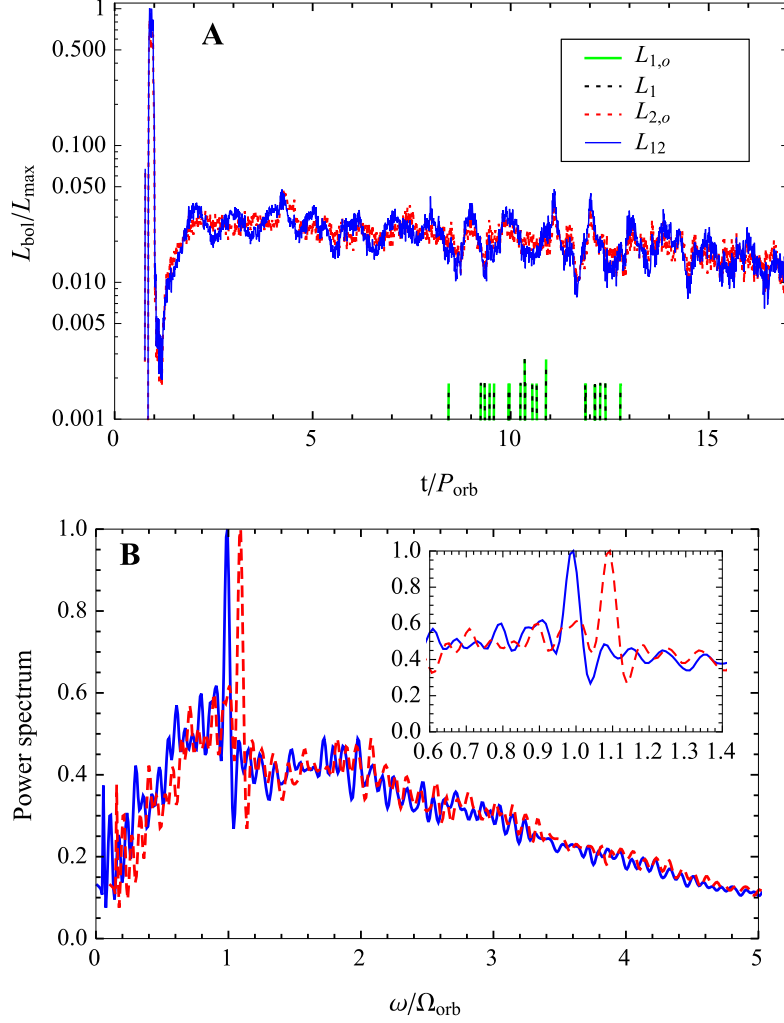


Fig. 3.— **(A)** Bolometric luminosity of the primary (red and blue) and secondary (black and green) black holes normalized by its maximum value L_{max} . The blue and black lines include relativistic beaming. **(B)** Power Spectrum of the bolometric light curves with relativistic beaming as a function of frequency ω in units of $\Omega_{\text{orb}} = 2\pi/P_{\text{orb}}$. The blue solid line shows the power spectrum of the first TDE, and the red dashed line shows that of the second TDE 50 years later. The half maximum full-width are given by 0.02858 ± 0.00158 with a fixed peak position 0.99251. If the two peaks are sampled by N data points, it should be possible to separate them even after a time interval of $50/\sqrt{N}$ years.

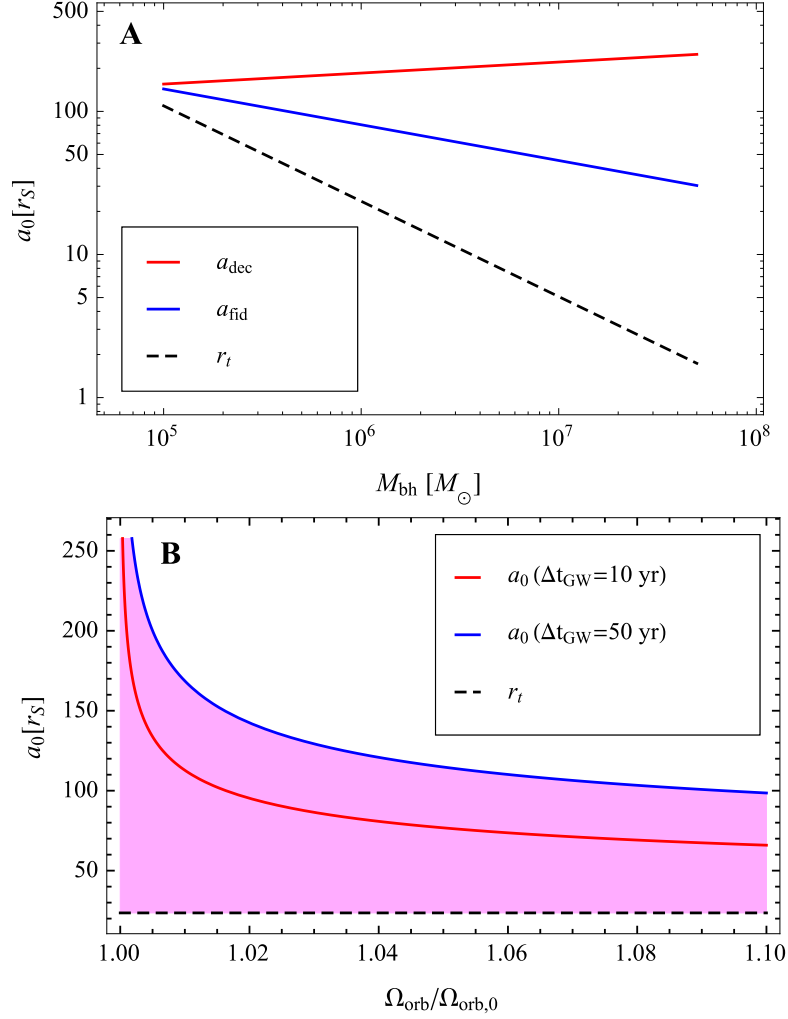


Fig. 4.— (A) Dependence of the decoupling radius on black hole mass. The red, blue and black dashed lines show the decoupling radius, fiducial semi-major axis, and tidal disruption radius, respectively. (B) Dependence of the semi-major axis at the first TDE, a_0 , on the orbital frequency at the second TDE, normalized by the orbital frequency at the first TDE, for $M_{\text{BH}} = 10^6 M_\odot$. The blue and red solid lines show a_0 if the time difference between the first and second TDEs is given by 10 and 50 years, respectively (see equation 8). The black dashed line shows the tidal disruption radius r_t below which the binary can be regarded as a single black hole (see equation 1).

Acknowledgments

The authors are grateful to Nicholas Stone for his helpful discussions. The numerical simulations were performed using a high performance computing cluster at the Korea Astronomy and Space Science Institute. This work was supported in part by the research grant of the Chungbuk National University in 2015 [K.H.] and by NSF grant AST-1312034 [A.L.].

REFERENCES

- Amaro-Seoane, P., Brem, P. & Cuadra, J. 2013, *ApJ*, 764, 14
- Artymowicz, P., & Lubow, S.H. 1994, *ApJ*, 421, 651
- Bate, M. R., Bonnel, I. A., & Price, N. M., 1995, *MNRAS*, 277, 362
- Balbus, S. A. & Hawley, J. F. 1991, *ApJ*, 376, 214
- Begelman, M. C., Blandford, R. D. & Rees, M. J. 1980, *Nature*, 287, 307
- Bloom, J. S. et al., 2011, *Science*, 333, 203
- Burrows, D. N. et al., 2011, *Nature*, 476, 421
- Chen, X., Madau, P., Sesana, A. & Liu, F. K. 2009, *ApJ*, 697, L149
- Chen, X., Sesana, A., Madau, P., & Liu, F. K., 2011, *ApJ*, 729, 13
- Colpi, M. & Dotti, M. 2011, *Advanced Science Letters*, 4, 181
- Donley, J. L., Brandt, W. N., Eracleous, M. & Boller, T. 2002, *AJ*, 124, 1308
- D’Orazio, J. D., Haiman, Z., & MacFadyen, A. 2013, *MNRAS*, 436, 2997
- D’Orazio, D. J., Haiman, Z. & Schiminovich, D. 2015, *Nature*, 525, 351
- Evans, C. R. & Kochanek, C. S. 1989, *ApJ*, 346, L13
- Farris, B. D., Duffell, P., MacFadyen, A. I., & Haiman, Z. 2015, *MNRAS*, 447, L80
- Gammie, C. F. 2001, *ApJ*, 553, 174
- Genzel, R. et al., 2003, *Nature*, 425, 934
- Gezari, S. et al., 2012, *Nature*, 485, 217

- Gongjie, Li., Smadar, N., Kocsis, B. & Loeb, A. 2015, MNRAS, 451, 1341
- Graham, M. J. et al., 2015, Nature, 518, 74
- Hayasaki, K., Mineshige, S. & Sudou, H. 2007, PASJ, 59, 427
- Hayasaki, K., Stone, N. & Loeb, A. 2013, MNRAS, 434, 909
- Ivanov, P. B., Polnarev, A. G. & Saha, P. 2005, MNRAS, 358, 1361
- Jiang, Y., Stone, J. M. & Davis, S. W. 2014, ApJ, 796, 106
- Komossa, S. & Greiner, J. 1999, A&A, 349, L45
- Kormendy, J. & Richstone, D. 1995, ARA&A, 33, 581
- Kormendy, J. & Ho, L. C. 2013, ARA&A, 51, 511
- Levan, A. J. et al., 2011, Science, 333, 199
- MacFadyen, A. I. & Milosavljević, M. 2008, ApJ, 672, 83
- Magorrian, J., et al., 1998, AJ, 115, 2285
- Mayer, L., Kazantzidis, S., Madau, P., Colpi, M., Quinn, T. & Wadsley, J. 2007, Science, 316, 1874
- Milosavljević, M. & Phinney, E. S. 2005, ApJ, 622, L93
- Miralda-Escudé, J. & Kollmeier, J. A. 2005, ApJ, 619, 30
- Miyoshi, M. et al., 1995, Nature, 373, 127
- Murray, D. C., & Dermott, S. F. 1999, *Solar System Dynamics* (Cambridge: Cambridge University Press), ch.3, 70
- Nayakshin, S., Cuadra, J. & Volker, S. 2007, MNRAS, 379, 21
- Ostriker, E. C. 1999, ApJ, 513, 252
- Paczynski, B. 1978, Acta Astron., 28, 91
- Peters, P. C. 1964, PRD, 136, 1224
- Rees, M. J. 1988, Nature, 333, 523
- Schödel, R., et al., 2002, Nature, 419, 694

- Sillanpää, A., Haarala, S., Valtonen, M. J., Sundelius, B. & Byrd, G. G. 1988, ApJ, 325, 628
- Velzen, S. & Farrar, G. R. 2014, ApJ, 792, 53
- Wang, J. & Merritt, D. 2004, ApJ, 600, 149
- Wegg, C. & Bode, J. N. 2011, ApJ, 738, L8
- Wetzel, A. R., Cohn, J. D., White, M. 2009, MNRAS, 395, 1376
- Zauderer, B. A. et al., 2011, Nature, 476, 425